AUGUST 28 2008

Direct measurement of sediment sound speed in Shallow Water '06

Jie Yang; Dajun Tang; Kevin L. Williams

J. Acoust. Soc. Am. 124, EL116–EL121 (2008)
https://doi.org/10.1121/1.2963038

Direct measurement of sediment sound speed in Shallow Water '06

Jie Yang, Dajun Tang, and Kevin L. Williams
Applied Physics Laboratory, University of Washington, 1013 NE 40th Street, Seattle, Washington 98105-6698
jieyang@apl.washington.edu, djtang@apl.washington.edu, williams@apl.washington.edu

Abstract: Knowledge of sediment sound speed is crucial for predicting sound propagation. During the Shallow Water '06 experiment, *in situ* sediment sound speed was measured using the Sediment Acoustic-speed Measurement System (SAMS). SAMS consists of ten fixed sources and one receiver that can reach a maximal sediment depth of 3 m. Measurements were made in the frequency range 2–35 kHz. Signal arrival times and propagation distances were recorded, from which sediment sound speed was determined. Preliminary results from three deployments show that SAMS was capable of determining sediment sound speed with uncertainties less than 1.6%. Little dispersion in sediment sound speed was observed.

PACS numbers: 43.30.Pc, 43.30.Ma, 43.30.Xm [WC]
Date Received: March 26, 2008 **Date Accepted:** May 19, 2008

1. Introduction

Acoustic interaction with the sea bottom is, in many cases, an essential component of sound propagation in a shallow water waveguide. *In situ* geoacoustic properties of the seabed, however, are difficult to obtain. Since the 1950s, *in situ* direct measurements have been carried out to study the sediment geotechnical properties.[1] More recently, sediment geoacoustic properties have been measured within the surfacial layer in the frequency range 1–100 kHz using either manually buried acoustic systems (Refs. 2–4) or specially designed underwater mechanical systems. Refs. 5–8, from the latter category, present systems that can penetrate into the sediment through their own gravitational forces. The *In Situ* Sediment geoacoustic Measurement System (Refs. 5–7) is designed for *in situ* measurements within the topmost 30 cm while the acoustic lance (Ref. 8) has a maximum penetration depth of 5 m.

As part of the experimental effort in Shallow Water '06 (SW06), the Sediment Acoustic-speed Measurement System (SAMS) was used to directly measure the sediment sound speed. SAMS is driven into the seabed by a powerful vibrocore, which allows precise penetration depth up to 3 m with arbitrary step size. The ground truth measurements are valuable not only in studying *in situ* sediment properties but also in providing sediment geoacoustic data to which inversion results can be compared.

This paper is organized as follows. In Sec. 2, the analyses of calibration and sediment data are presented. Section 3 summarizes and discusses future directions. System uncertainty analysis is given in the Appendix.

2. Data analysis

SAMS was deployed during the SW06 field experiment. Four data sets, one in the water column as calibration and three in the sediment, were recorded. For all data sets, three linear-frequency-modulated (LFM) "chirps" were used in the frequency bands 2–11, 10–21, and 20–35 kHz, which are referred to as low-, mid-, and high-frequency (LF, MF, and HF) in later analysis.

2.1 Analysis of calibration data

Calibration data were acquired in a bay environment and relatively far from the positions of the sediment measurements. For calibration, SAMS was deployed such that both sources and re-

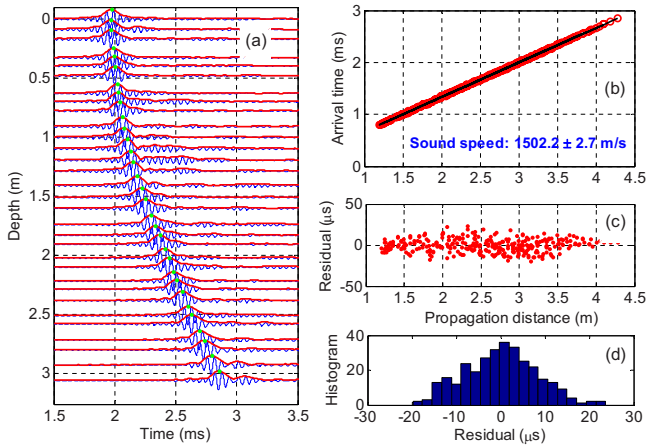

Fig. 1. (Color online) Pulse compression results at MF. (a) Waveforms received from source 10; (b) linear regression results; (c) linear regression residual scatter plot; (d) residual histogram.

ceiver were always within the water column. The analysis of the calibration data is used to augment the system geometry measurements and establish system uncertainty.

SAMS consists of a 3-m-tall triangular frame and a 2-m-long extension beam. Three sources are fixed on the triangular frame with the other seven on the extension beam. The receiver is located in the center of the frame and can be driven vertically into the sediment using a vibrocore. Horizontal distances between sources and receiver are between 1.18 and 2.97 m.

Data were taken at 31 receiver depths with a stepsize of about 0.1 m. At each depth, the ten sources sequentially transmitted three chirps and each was repeated five times. Pulse compression was carried out as an initial step in processing the data. In Fig. 1(a), pulse compressed waveforms received from source ten are plotted at their corresponding receiver depths. Signal arrival time is defined as the time at the peak of the envelope and highlighted with a dot. With signal arrival times defined, the speed of sound in water can be determined from the linear regression of the arrival times and distances between the sources and receiver. Five repeated pings are used to find the averaged arrival times yielding a total of 310 data points. The linear regression result, Fig. 1(b), is 1502.2 m/s with 2.7 m/s uncertainty at the 95% confidence level. The calculation of uncertainty assumes that the residuals (difference between data and fit function) are random and follow a normal distribution of zero mean and constant variance. A scatter plot of the residuals is shown in Fig. 1(c). Both the scatter plot and its histogram [Fig. 1(d)] indicate that the distribution of the residual is close to normal. Similar procedures are repeated for the LF and HF calibration data. The curve fitting results for the speed of sound in water are 1503.4±6.7 and 1503.1±3.4 m/s, respectively.

The sound speeds determined are close to each other with the confidence interval at MF and HF almost completely enclosed by that of the LF. The higher uncertainty at LF is due to a roughly 58% decrease in the total number of data points included in the curve fitting process. Beyond 2 m, the LF calibration data showed signals, possibly due to the tube waves, arriving prior to the direct arrivals and, therefore, were excluded from the curve fitting. Unfortunately, there was no conductivity-temperature-depth (CTD) record when the calibration data were taken. Concurrent ship data only provide temperature and salinity at the sea surface. Therefore, a total of 120 historical summer CTD data around the area were sought for reference. Individual distance to the SAMS calibration position varied from 16 to 52 km and water depth ranged 13–40 m. A strong thermocline was observed starting at around 10 m and water sound speed varied from 1520 m/s at the sea surface to 1495 m/s at 35 m. For calibration, bathymetry showed a 23 m water depth with SAMS suspended 5–6 m below the surface, i.e., measurements were taken at 6–9 m in depth. Compared with historical CTD data, the calibration results, 1503.4±6.7, 1502.2±2.7, and 1503.1±3.4 m/s, respectively, are reasonably within the

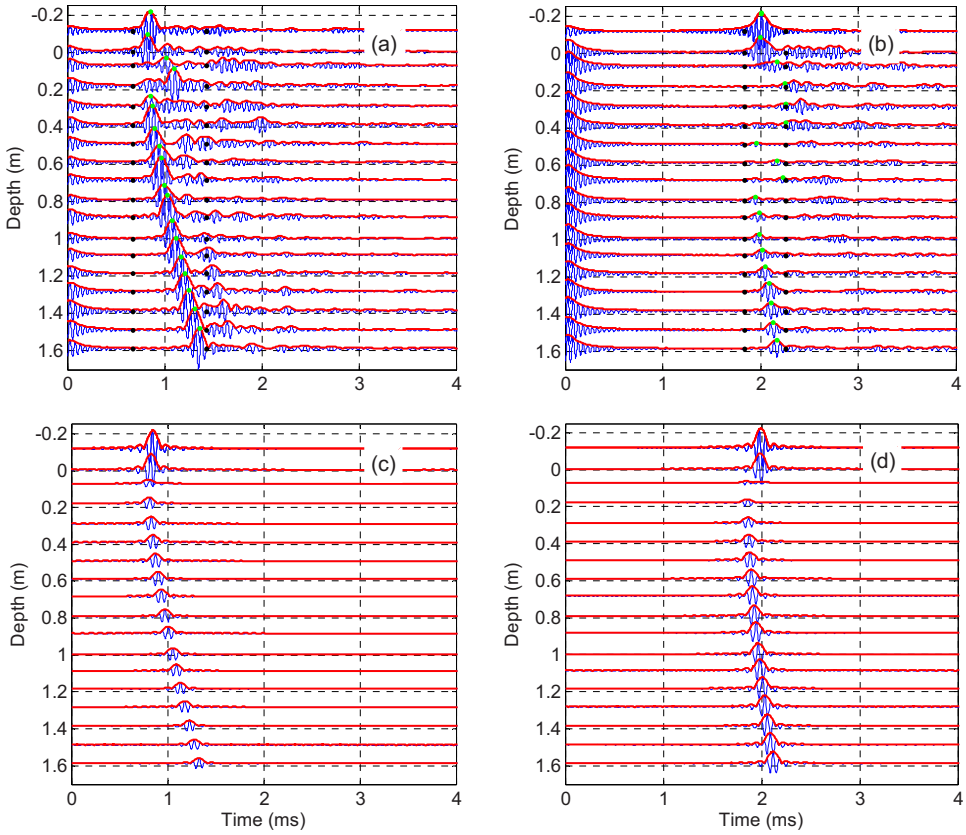

Fig. 2. (Color online) MF Pulse-compressed waveforms from: (a) source 1; (b) source 10 at different receiver depths. (c) and (d) are half-space Green's function simulations of (a) and (b), respectively.

variation range. More importantly, the acoustic data are of good quality and repeatable at different frequency bands, supporting the conclusion that the water sound speeds measured by SAMS are close to the true values at the time.

2.2 Analysis of sediment data

To start, two cases in the MF band from position 2 are chosen to show the characteristics of sediment data. The first case, Fig. 2(a), draws the signals from source 1 at 19 receiver depths with the maximum penetration depth around 1.6 m. Data are processed in the same way as the calibration. The receiver starts at about 10 cm above the sediment surface, which makes the first depth sample less than zero in the figure. In determining the signal arrival time, a time window is specified (bounded by the black dots) within which the peak of the signal envelope is recognized and highlighted with a green dot. It is quite obvious that there are two erroneous readings of the peak time in Fig. 2(a) as the receiver first enters the sediment. For sources that are further away from the receiver, there are more such occurrences as shown in Fig. 2(b). Data of this kind are carefully excluded from analysis. Signal-to-noise ratio drops considerably for the geometries realized in Fig. 2(b) due to the combined effects of longer acoustic path through the sediment and ray bending by the critical angle. A two-half space Green's function is used to simulate the scenario of Figs. 2(a) and 2(b) and the results are shown in Figs. 2(c) and 2(d). The critical angle effect is quite apparent in Fig. 2(d).

Table 1. Summary of sediment sound speed results.

		C_b (m/s)
Position 1	LF	1614.8 ± 8.7
	MF	1622.1 ± 12.5
Position 2	LF	1597.7 ± 11.0
	MF	1598.6 ± 9.8
Position 3	LF	1588.2 ± 15.8
	MF	1611.6 ± 24.8

To find sediment sound speed, the water sound speed close to the water–sediment interface is required. Throughout the experiment, CTD records show a very stable water sound speed at depths beyond 70 m. Based on CTD records, the water sound speed is 1496 m/s. Sediment sound speed is assumed homogeneous within the penetrated depth, 1.6 m. Ray tracing is carried out for each data point by varying sediment sound speed in the model and the closest match of arrival times between measurement and ray tracing determines the *in situ* sediment sound speed. The uncertainties are determined in the same manner as for the calibration (Sec. 2.1). Assuming uncertainty comes entirely from propagation in the sediment, the time and distance that are spent in water are removed from the total time and distance. The uncertainty in sediment sound speed is then calculated using the residuals at 95% confidence level.

Results are summarized in Table 1 and Fig. 3. Results from positions 1 and 2 show similar uncertainty bounds around 10 m/s and little dispersion between the two frequency bands. There is about a 20-m/s sound speed difference between the two positions, which is believed to be the true spatial variation. Results at position 3 have much larger uncertainties than the other two. Signs of signal degradation were observed (not shown here), which results in a 50% higher mean residual than the other two positions. Geological studies around the SW06 region (Ref. 9), using interpreted chirp seismic reflection data, indicate a substantial difference in sediment properties at position 3 from positions 1 and 2, which is believed to be the cause for higher uncertainty at position 3. In addition, acoustic measurements of bottom reflection (Ref. 10) were made in the vicinity of SAMS positions 1 and 2 in the frequency range 1–20 kHz. The geoacoustic inversion results of sediment sound speed, with co-located coring and stratigraphic studies, are consistent with the direct measurement results using SAMS.

3. Summary and future directions

In this paper, direct measurements of sediment sound speed using the Sediment Acoustic-speed Measurement System (SAMS) have been presented. The calibration data were first analyzed to establish the system uncertainty, which is approximately 3 m/s. Sediment data were taken at three positions. Sediment sound speeds and uncertainties are summarized in Table 1 and Fig. 3. Results indicate a 20-m/s sound speed variation between positions 1 and 2. At position 3, the

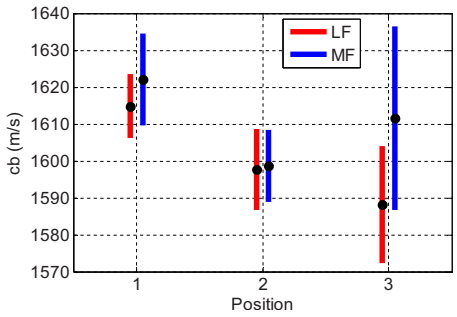

Fig. 3. (Color online) Sediment sound speeds with uncertainties at three positions.

increase in uncertainty may be attributed to the sediment properties based on geological studies around the central experimental area in SW06. The sediment sound speeds found at positions 1, 2, and 3 are 1618 ± 11, 1598 ± 10, and 1600 ± 20 m/s, respectively. Little dispersion in sediment sound speed was observed. Direct measurement of sediment sound speed dispersion has been found in sandy sediments (Refs. 2 and 11). The dispersion was observed to be at its greatest in the frequency range 800–2000 Hz. In this work, the frequency coverage is higher than the pronounced transition region of dispersion, which may explain the observed lack of dispersion. Future directions include improvement of system uncertainty in sediment sound speed, determination of sediment attenuation and its dispersion relation, and depth dependence of sediment geoacoustic properties.

Acknowledgment

This work was supported by the Office of Naval Research.

Appendix: System uncertainty analysis

For a system like the SAMS, the dimension and propagation time uncertainties limit the resolution of sound speed measurement. Uncertainty can come from both measurements and methodology utilized to analyze data. In this work, part of the uncertainty comes from measurement of distances, i.e., horizontal distance and initial depth offset between sources and receiver; initial depth offset between receiver and the sediment surface; and receiver depth reading. The reading of the arrival times falls in the latter category.

Following Ref. 12, a general function q with multiple variables $(x, y, z, \ldots)$ has uncertainty:

$$\delta q = \sqrt{\left(\frac{\partial q}{\partial x}\delta x\right)^2 + \left(\frac{\partial q}{\partial y}\delta y\right)^2 + \left(\frac{\partial q}{\partial z}\delta z\right)^2 + \cdots}. \tag{A1}$$

In Eq. (A1), variables $x, y, z, \ldots$ are independent measurements with uncertainties $\delta x, \delta y, \delta z, \ldots$. For this work, the general function is the speed of sound in water, c_w, which is the ratio of distance and time:

$$c_w = \frac{r(x,y,z,\cdots)}{t} = \frac{\sqrt{x^2 + (h+d)^2}}{t}, \tag{A2}$$

where r is the slant distance, t is travel time; x, h, and d are horizontal distance, receiver depth, and initial vertical distance between source and receiver. Following Eq. (A1), the uncertainty in calibration can be written as

$$\delta c_w = \sqrt{\left(\frac{\partial c_w}{\partial x}\delta x\right)^2 + \left(\frac{\partial c_w}{\partial h}\delta h\right)^2 + \left(\frac{\partial c_w}{\partial d}\delta d\right)^2 + \left(\frac{\partial c_w}{\partial t}\delta t\right)^2}. \tag{A3}$$

The individual uncertainties $\delta x, \delta h, \delta d$ are defined as 0.9, 0.1, and 0.5 cm. Specifically, δx is set to $\frac{1}{4}$ of the source dimension; δd is set to $\frac{1}{4}$ of the receiver dimension; δh accounts for depth reading uncertainty. In Eq. (A3), the most difficult part is to determine δt. The receiver is embedded inside a stainless steel tube with two rectangular windows open on the side. The combination of direct arrival and reflections off the window may slightly change the location of the signal peak. Assuming this window effect is random, δt can be determined using the mean residual obtained from Fig. 1 as 7.5 μs. Figure 4 shows the uncertainty corresponding to each source. For each of them, as depth increases, the uncertainty decreases from top to bottom. The black dashed line is the mean value for each source. It is obvious that sources that are closer to the receiver have higher uncertainty and spreading. The least uncertainty for an individual measurement is around 5 m/s.

In calibration analysis, data recorded from all ten sources were used in the linear regression to find the speed of sound in water, i.e., a relationship between individual (Fig. 4) and overall uncertainty (Fig. 1) needs to be clarified. The overall system uncertainty can be deter-

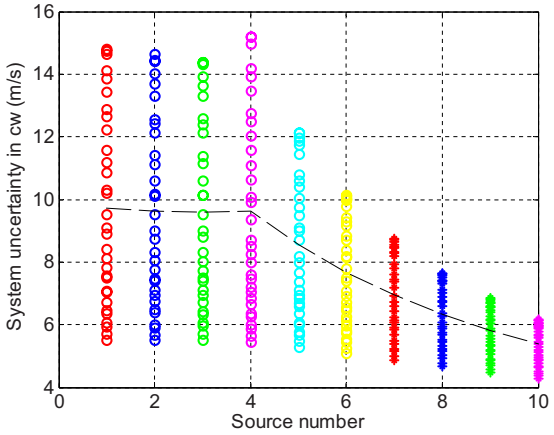

Fig. 4. (Color online) System uncertainty in the speed of sound in water.

mined from the individual uncertainties in Fig. 4 as a two-step process. First, assume an ideal system with no uncertainty, i.e., find propagation times by dividing measured propagation distances by a fixed sound speed. The value c_w=1502.2 m/s, determined from calibration at MF, is used. The linear regression shows a perfect fit between propagation distance and time with zero uncertainty. Second, convert the maximum uncertainty of each source δc_w, as in Fig. 4, to its equivalent uncertainty in distance, i.e., by multiplying δc_w with corresponding propagation time t. Then, the measured propagation distances were added a random quantity in the range of $\pm t \times \delta c_w$. The linear regression is carried out again by forcing c_w=1502.2 m/s. The system uncertainty at 95% confidence interval is calculated in a similar fashion as in Sec. 2. This uncertainty, determined to be ±1.6 m/s, is the overall system uncertainty.

References and links

[1]E. L. Hamilton, G. Shumway, H. W. Menard, and C. J. Shipek, "Acoustic and other physical properties of shallow-water sediments off San Diego," J. Acoust. Soc. Am. **28**, 1–15 (1956).
[2]A. Turgut and T. Yamamoto, "Measurements of acoustic wave velocities and attenuation in marine sediments," J. Acoust. Soc. Am. **87**, 2376–2383 (1990).
[3]A. I. Best, Q. J. Huggett, and A. J. K. Harris, "Comparison of in situ and laboratory acoustic measurements on Lough Hyne marine sediments," J. Acoust. Soc. Am. **110**, 695–709 (2001).
[4]G. B. N. Robb, A. I. Best, J. K. Dix, P. R. White, T. G. Leighton, J. M. Bull, and A. Harris, "Measurements of the in situ compressional wave properties of marine sediments," IEEE J. Ocean. Eng. **32**, 484–496 (2007).
[5]A. Barbegelata, M. D. Richardson, B. Miaschi, E. Muzi, P. Guerrini, L. Troiano, and T. Akal, "ISSAMS: An in situ sediment acoustic measurement system," in *Shear Waves in Marine Sediments*, edited by J. M. Hoven, M. D. Richardson, and R. D. Stoll (Kluwer, Dordrecht, 1991).
[6]M. D. Richarson, D. L. Lavoie, and K. B. Briggs, "Geoacoustic and physical properties of carbonate sediments of the lower Florida Keys," Geo-Mar. Lett. **17**, 316–324 (1997).
[7]M. J. Buckingham and M. D. Richardson, "On tone-burst measurements of sound speed and attenuation in sandy marine sediments," IEEE J. Ocean. Eng. **27**, 429–453 (2002).
[8]S. S. Fu, R. H. Wilkens, and L. N. Frazer, "Acoustic lance: New in situ seafloor velocity profiles," J. Acoust. Soc. Am. **99**, 234–242 (1996).
[9]J. A. Goff, B. J. Kraft, L. A. Mayer, S. G. Schock, C. K. Sommerfield, H. C. Olson, S. P. S. Gulick, and S. Nordfjord, "Seabed characterization on the New Jersey middle and outer shelf: Correlatability and spatial variability of seafloor sediment properties," Mar. Geol. **209**, 147–172 (2004).
[10]J. W. Choi, P. H. Dahl, and J. A. Goff, "Observations of the R reflector and sediment interface reflection at the Shallow Water '06 Central Site," J. Acoust. Soc. Am. **124**, EL128–EL134 (2008).
[11]K. L. Williams, D. R. Jackson, E. I. Thorsos, D. Tang, and S. G. Schock, "Comparison of sound speed and attenuation measured in a sandy sediment to predictions based on the Biot theory of porous media," IEEE J. Ocean. Eng. **27**, 413–428 (2002).
[12]J. R. Taylor, *An Introduction to Error Analysis*, 2nd ed. (University Science Books, 1997).